

Mid Infrared Photometry of Mass-Losing AGB Stars.

M Busso ¹

Department of Physics, University of Perugia, via Pascoli, Perugia, Italy, 06123;
busso@fisica.unipg.it

R. Guandalini¹

Department of Physics, University of Perugia, via Pascoli, Perugia, Italy, 06123;
guandalini@fisica.unipg.it

P. Persi ²

INAF, Istituto di Astrofisica Spaziale e Fisica Cosmica, via Fosso del Cavaliere, 00100
Roma, Italy; persi@iasf-rm.inaf.it

L. Corcione³

INAF, Osservatorio Astronomico di Torino, via Osservatorio 20, 10025 Pino Torinese, Italy;
corcione@oa-torino.inaf.it

and

M. Ferrari-Toniolo²

INAF, Istituto di Astrofisica Spaziale e Fisica Cosmica, via Fosso del Cavaliere, 00100
Roma, Italy; ferrari@iasf-rm.inaf.it

Received _____; accepted _____

ABSTRACT

We present ground-based mid-infrared imaging for 27 M-, S- and C-type Asymptotic Giant Branch (AGB) stars. The data are compared with those of the database available thanks to the IRAS, ISO, MSX and 2MASS catalogues. Our goal is to establish relations between the IR colors, the effective temperature T_{eff} , the luminosity L and the mass loss rate \dot{M} , for improving the effectiveness of AGB modelling. Bolometric (absolute) magnitudes are obtained through distance compilations, and by applying previously-derived bolometric corrections; the variability is also studied, using data accumulated since the IRAS epoch. The main results are: i) Values of L and \dot{M} for C stars fit relations previously established by us, with Miras being on average more evolved and mass losing than Semiregulars. ii) Moderate IR excesses (as compared to evolutionary tracks) are found for S and M stars in our sample: they are confirmed to originate from the dusty circumstellar environment. iii) A larger reddening characterizes C-rich Miras and post-AGBs. In this case, part of the excess is due to AGB models overestimating T_{eff} for C-stars, as a consequence of the lack of suitable molecular opacities. This has a large effect on the colors of C-rich sources and sometimes disentangling the photospheric and circumstellar contributions is difficult; better model atmospheres should be used in stellar evolutionary codes for C stars. iv) The presence of a long-term variability at mid-IR wavelengths seems to be limited to sources with maximum emission in the $8 - 20 \mu\text{m}$ region, usually Mira variables (1/3 of our sample). Most Semiregular and post-AGB stars studied here remained remarkably constant in mid-IR over the last twenty years.

Subject headings: Stars: mass-loss – Stars: AGB and post-AGB – Stars: carbon – Stars: Mira – Infrared: stars

1. Introduction

Stars of low and intermediate mass (all those below $M = 7\text{--}8 M_{\odot}$) terminate their evolution through the so-called Asymptotic Giant Branch (AGB) phase [Busso et al. 1999; Busso 2007], in which they lose mass efficiently thanks to stellar winds powered by radiation pressure on dust grains [Habing 1996]. After this stage, they generate planetary nebulae and start a blue-ward path, which ultimately gives birth to a white dwarf [see also Herwig 2005].

While moving along this path, AGB stars replenish the Interstellar Medium with about 70% of all the matter returned after stellar evolution [Sedlmayr 1994]; this is done through the formation of extended circumstellar envelopes [Winters et al. 2002]. Cool or cold dust, with its radiative emission in the infrared (IR), normally dominates the energy distribution of these sources, so that until recently the bolometric (apparent) magnitude of the most evolved AGB stars was difficult to derive, due to insufficient photometric coverage of the mid-far IR range of the electromagnetic spectrum. Traditionally, circumstellar envelopes were studied using fluxes provided by the IRAS satellite [see Jura 1986; Jura & Kleinmann 1989], which had however a poor spatial resolution (hence some risk of contamination, especially at the longest wavelengths). Similarly, absolute magnitudes were very uncertain due to the difficulties in measuring the distance of these single, strongly variable stars.

Only recently, the availability of a large IR database from space-borne telescopes like ISO, IRTS, MSX and the increased amount of ground-based mid-IR observations have substantially modified the situation. The quantitative studies of luminosities, colors and mass loss in the last evolutionary stages of moderately massive stars have consequently grown in number and quality [Whitelock et al. 2006; Feast et al. 2006]. In parallel, Hipparcos distances for AGB stars have been in part upgraded [Bergeat & Chevallier 2005]. The results may still include inconsistencies (Feast, private communication) but a full revision of the

Hipparcos catalogue is still waited for [van Leeuwen 2005; van Leeuwen & Fantino 2005]. Recent works have therefore largely exploited Period-Luminosity relations to infer the distances [Menzies et al. 2006; Feast 2007]. Contemporarily, the first results of Spitzer’s surveys are becoming available [Zijlstra et al. 2006].

In the above modified scenario we started a reanalysis of galactic AGB stars at IR wavelengths, aimed at improving the determination of their energy distribution, mass loss and absolute magnitudes, making use of recent IR photometric data and of reliable distance estimates. With such works one can now finally compare homogeneous samples of mass losing stars in the Galaxy with similar data sets in Magellanic Clouds [van Loon et al. 2001; van Loon et al. 2005], in order to study the dependence on metallicity of general stellar properties.

In a previous paper [Guandalini et al. 2006, hereafter Paper I] we considered C stars as observed by the ISO-SWS and by the MSX experiments. Here we extend our work by analyzing a sample of 27 AGB stars of classes M, S and C (listed in Table 1) for which we obtained ground-based infrared imaging in the 10 μm window. Most of the stars we observed were also the object of measurements by the above quoted space-borne IR telescopes, so that we can now compare and integrate results from different experiments and different epochs, as a check of the quality of the available infrared database and of the source variability.

This paper is organized as follows: in section 2 we briefly discuss our IR camera, used for making the ground based observations. In section 3 we present the photometric data obtained through it at wavelengths longer than 8 μm , integrated by the near-IR archive observations of 2MASS [Cutri et al. 2003] and by the available estimates for mass loss rates, distances and a few other relevant parameters. In section 4 we then use the database thus constructed to derive bolometric magnitudes (both apparent and absolute), colors, and

correlations of photometric properties with mass loss rates. Then section 5 addresses the long-term variability issue, by going back to the IRAS catalogues in order to compare the available data over a time interval of about 20 years. Finally, in section 6 we outline some general conclusions, underlining the main remaining problems that remain to be solved for allowing a satisfactory match between photometric observations and stellar modelling.

2. The Mid-IR Camera TIRCAM2 and its Calibration

Our sample stars were observed between 2001 and 2004 at the Italian Infrared telescope (TIRGO), located at 3200 meters over the sea level, on top of the Gornergrat, in Switzerland. The data were collected using our mid infrared camera TIRCAM2 (Tirgo Infrared Camera - version 2), an upgrade of a previously available instrument [Persi et al. 1994].

TIRCAM2 uses a Rockwell (then Boeing) high-flux Si:As BIB 128×128 array (HF-21) and is equipped with five narrow-band filters (10% bandwidth) between 8 and $13 \mu\text{m}$, with the N broad-band filter, and with a circular variable filter (CVF) having a spectral resolution of 3% in the 8-14 μm range. The optics of the camera produce a plate scale at TIRGO of $0.77''/\text{pix}$. The array, the optical system and the filters are assembled in a liquid-He-cooled dewar (HD-3[8]) of the Infrared Labs. Inc. (Tucson, Arizona). The readout electronics of the array, fully developed by our home Institutes, and the other general characteristics of the instrument have been previously described elsewhere [Persi et al. 2002; Corcione et al. 2003]. The absolute fluxes of some infrared standard stars in our photometric system are shown in Table 2. They have been derived from the spectral energy distributions (SEDs) published by Cohen and coworkers [Cohen et al. 1999, and references therein], after a convolution with the spectral response of our filters [Persi et al. 2002].

The narrow-band images at 8.8, 9.8, 11.7 and 12.5 μm of our sample of AGB stars were taken in the standard chopping & nodding technique, in order to remove the sky and telescope emission background. Images of standard stars were obtained during the nights at similar air mass as our targets, for flux calibration. They were also used to estimate the point-spread function (PSF) at each wavelength. The mean PSF (FWHM) obtained during our observing runs was $\sim 3.2''$ in diameter at 8.8 μm and $\sim 3.8''$ at 12.5 μm . All the observed AGB stars appear as point-like sources at this spatial resolution. The on-source integration times were from 720sec for the faintest sources, down to 120sec for the brightest ones, in all the filters used. The derived detection limit is approximately 0.7 Jy (1σ) in 300sec of integration time. The photometric measurements were extracted from the images of AGB stars through the DAOPHOT tool, within the IRAF data reduction package [Stetson 1987], using an aperture of $6''$.

3. Infrared Colors and Mass Loss of AGB Sources

The flux densities of the sources observed, as measured with the technique mentioned in the previous section, are given in Table 3, together with their 1σ statistical errors. We collected, as a comparison, near infrared fluxes for our sources, as published in the 2MASS catalogue, together with observations by the MSX satellite (when available) for wavelengths longer than those of our filters. These data are presented in Table 4. Finally, distances, mass loss rates and wind velocities, as deduced by the literature, are presented in Table 5, together with the relevant references.

By calibrating the data of Table 3 with the zero-magnitude fluxes deduced by standard stars in Table 2, we obtain the infrared colors of the sources. Examples of color-color diagrams are shown in Figure 1 and in Figure 2. Here TIRCAM2 sources are represented by big symbols: open-starred ones refer to M-type (oxygen-rich) stars, plain open ones to

S-type stars. Filled symbols indicate C-rich sources. Small dots refer to the sample of C stars we discussed in Paper I, with colors deduced from ISO and MSX observations, as a comparison (see Figure 6 in Paper I). We recall that the ISO data were taken from the last on-line database available, where SWS measurements are fully calibrated [Leech et al. 2004]. From them we derived photometric estimates in the TIRCAM2 photometric system by convolving SWS spectra with the response curves of our filters (see Paper I).

The bulk of our data is generally distributed along the line of black body emission in Figure 1, while a larger dispersion is present in Figure 2.

The spread in Figure 2 derives from the fact that, for sources that are presently on the AGB (Semiregulars or Miras), color indexes computed in the $8 - 14\mu\text{m}$ region are affected by the crowding of variable emission (or absorption) features characteristic of these wavelengths (e.g. at $11.2 - 11.7\mu\text{m}$ for C-stars, from PAH and SiC; and at $9.8\mu\text{m}$ for O-rich sources, from silicates). When colors outside the $8 - 14\mu\text{m}$ band are used (Figure 1) excess emission at $21\mu\text{m}$ is seen for a number of post-AGB, C-rich TIRCAM2 sources (as also shown by ISO and MSX data, see Paper I). Emission at this wavelength was known to be a distinctive property of a few post-AGB C stars and C-rich pre-planetary nebulae [Kwok et al. 2002; Zhang et al. 2006]. However, so far the number of known sources with this feature was rather limited: in our data (both here and in Paper I) the $21\mu\text{m}$ emission appears as a general property of post-AGB sources. The above simple considerations confirm the fact that mid-IR colors are effective tools for classifying AGB sources. When one deals with infrared stars, mid-IR colors identify C-rich AGBs through their color excess at $11.7\mu\text{m}$, and C-rich post-AGBs through their $21\mu\text{m}$ excess.

Figure 3 then shows the relations linking the IR colors to mass loss. Again, the best measurements selected for C stars in Paper I are included for comparison. It is clear that our new C-star data follow the trends already established, as expected. It is however also

evident that the (few) O-rich sources of the sample behave differently, displaying lower mass-loss rates for a given value of the color, especially when this last makes use of fluxes in the $10\mu\text{m}$ region (panel "a" in Figure 3). Should this hint be confirmed, this would mean that the relation between dust opacities and mass loss rates for M and S stars has to be different than for C-stars. We are now verifying this in a dedicated work on a much larger database (Guandalini & Busso in preparation).

4. Color-magnitude Diagrams and Effective Temperatures

By applying to our database the bolometric corrections discussed in Paper I, we can easily derive apparent bolometric magnitudes of the C-rich sources studied. For O-rich S and M stars we applied instead the bolometric correction [Guandalini et al. 2007]:

$$M_{bol} - M[8.8] = ax^3 + bx^2 + cx + d \quad (1)$$

where x is the K-[8.8] color, and the coefficients are $a=-0.0211$, $b=0.0812$, $c=1.0658$, $d=2.3026$ (with a correlation $r^2 = 0.989$). Correcting for the distance (see Table 5) yields the absolute bolometric magnitude, through which the absolute color-magnitude diagram can be plotted. Examples are presented in Figures 4 and 5.

In Figure 4 the dashed area represents the zone occupied by AGB photospheres according to current stellar models [Straniero et al. 1997]. As the Figure shows, essentially all the stars of our sample, much like those of Paper I, are reddened with respect to the models, by amounts that are widely disperse. Especially for the reddest stars, the displacements are dominated by the known presence of dust in the circumstellar envelope. In this respect, an additional source of concern is however introduced by the poor knowledge of molecular opacities for C-rich atmospheres, and by the fact that they are usually neglected in stellar codes [Marigo et al. 1998]. Due to this, it is known that the model

effective temperatures of very cool, C-rich AGB models, in the region of thermal pulses, are unreliable and generally largely overestimated. For strongly variable, dynamically perturbed atmospheres the same physical meaning of T_{eff} becomes doubtful [Uttenthaler et al. 2007].

Uncertainties in model T_{eff} values have very different consequences on the colors of M-type and C-type stars. As an example, let's consider, for AGB stars of the two classes, the effects of a change by 0.1 dex in $\log T_{eff}$. For M stars this corresponds e.g. to moving from type M3 to type M8: the (J-K) color difference in Figure 4 is less than 0.2mag. On the contrary, using for C stars the classifications and the color calibrations by Bergeat et al. (2001), we see that the same shift, corresponding e.g. to moving from the class CV6 to the class CV7 [Bergeat et al. 2002], may imply a color difference (J-K) $\simeq 1$ [see Figure 4 in Bergeat et al. 2001]. Similar considerations would hold for the [K-12.5] color in Figure 5. We conclude that, while the colors of O-rich AGB stars are not significantly affected by uncertainties in the atmospheric models, for C-stars the situation is worse. At least the less reddened stars in Figure 4 might show displacements from the model areas partly due to the real presence of dust, but partly also induced by errors in model T_{eff} values, hence in atmospheric opacities.

A special word of caution must be added for the positions of post-AGB objects in the two plots discussed here. Sometimes they have a complex SEDs, related to the fact that the central star begins to be detached from the circumstellar shell and shines at a relatively high temperature, as typical of a yellow supergiant. In such cases the integral of the IR flux (and in general the procedure described in Paper I) is not sufficient to determine the bolometric magnitude properly, because the optical contribution is not negligible [see e.g. Kwok et al. 1999, Fig. 1]. For post-AGB objects we have therefore only lower limits to the bolometric magnitudes, which approximate the real values with an error that is different for different cases.

In order to illustrate the cautious remarks made above for the relations between the color excess and the presence of dust, we selected in our sample of TIRCAM2 sources, and in the "best set" of sources in Paper I (those with astrometric distances and very detailed SEDs up to beyond $40\ \mu\text{m}$) a group of stars for which independent estimates of T_{eff} exist [Olofsson et al. 1993a; Olofsson et al. 1993b; Bergeat et al. 2001] or can be inferred from published color calibrations [Bessell et al. 1998]. For these objects we plot the absolute HR diagram (M_{bol} versus T_{eff}) in Figure 6. In the Figure, the tracks on the left refer to AGB models for various masses and metallicities [Straniero et al. 2003]. It is evident that, while the observed magnitudes fall in the range expected by these calculations (which include minimal or no overshooting), a large number of sources, and in particular the C-rich ones, have temperatures much lower than those predicted: these last, lacking a treatment for C-rich molecular opacities, can be in error by up to 30%.

The effects of absorption features from molecules like CO, CN and C_2 was shown to be extremely sensitive to the effective temperature and of large consequence for the near infrared colors by an hydrostatic analysis of a few C stars [Loidl et al. 2001]. The influence of molecular opacities for the changing composition of AGB envelopes gradually enriched by the TDU process, and in particular for C-rich sources, was also addressed by Marigo (2006). She showed how a large decrease in T_{eff} can be induced by the inclusion of opacities from molecules made of CNO and hydrogen. In models of about $2\ M_{\odot}$ a shift in $\text{Log } T_{eff}$ of almost 0.1 dex can be obtained (see Figure 6 in that paper). Just as an example, by reducing of this amount the temperatures of the model tracks in Figure 6 (in order to simulate the effect of molecular opacities) we get the curves at the right side of the plot (those with crosses superimposed). It is evident that a proper atmospheric model might be in many cases sufficient to yield the values of T_{eff} derived from observations. We warn that the new tracks must be seen only as a rough example, plotted for illustration purposes. In fact, Marigo (2006) computed a synthetic AGB evolution (while the tracks

in Figure 6 were derived from complete AGB models), and her assumptions for dredge-up were rather different than those in the models we used [Straniero et al. 2003]. What one would really need here is a set of complete AGB models, including a proper treatment of surface opacities for the changing envelope composition during the TDU process, something that unfortunately does not exist yet.

The above discussion says that, for C-stars, disentangling the atmospheric opacity effects from the color excess due to dust will become quantitatively meaningful only with large samples of good mid-IR observations, determining the properties of dust for sources where T_{eff} has been independently determined (e.g. from spectra). This in its turn would help stellar modelers to construct more detailed opacity tables, calibrated on observations. This is a relevant target to be pursued. In fact, the compilation of accurate infrared catalogues was started by several groups years ago [see for example van Loon et al. 1999; Cioni et al. 2001; Le Bertre et al. 2001]. It has continued to be an essential tool in recent years [Bergeat et al. 2002; Le Bertre et al. 2003; Cioni et al. 2003] and remains important now [Bergeat & Chevallier 2005; Le Bertre et al. 2005; Whitelock et al. 2006]. It will also be one of the key projects of the Antarctic telescope IRAIT (International Robotic Antarctic Infrared Telescope) that we recently developed and that will be operative at the Italo-French base of Dome C starting from the 2007-2008 Antarctic campaign [see e.g. Tosti et al. 2006; Busso et al. 2006].

5. Infrared Variability

Figures 7 and 8 show the available information on the IR SEDs for two groups of sources in the list of Table 1. The plots include data from the IRAS-PSC (Point Source Catalogue), IRAS-LRS (Low Resolution Spectra), ISO and MSX, together with our TIRCAM2 measurements. Figure 7 shows distributions that, despite their different

appearance, share the property of being non-variable over a time interval of almost 20 years. The figure contains rather heterogeneous measurements: photometric data (from the IRAS Point Source Catalogue, from MSX and from our ground-based observations) are compared with spectroscopic information from ISO-SWS and IRAS-LRS. For our purposes this is sufficient: as verified in Paper I, the proper convolution of ISO-SWS and IRAS-LRS spectra with the response of our filters, yielding a homogeneous photometric database, would not affect the flux levels by more than 5%, which is well inside the internal uncertainty of each set of data used. A constancy of the IR energy distribution is the more common behavior displayed by our sources, being shared by exactly 2/3 of the AGB stars in our sample (18 out of 27). This property characterizes stars that are very different from one another. They include sources with minimal IR excess (usually Semiregulars), in which the SED is peaked in near-IR; but they also include evolved (post-AGB) objects, in which the maximum emission is at very long wavelengths (from 20 to more than 40 μm), due the dominant effects of cold, distant dust.

In contrast, Figure 8 shows the behavior of intermediate objects, usually Mira variables, in which the emission peaks near 10 μm (and sometimes is rather flat up to about 20 μm), efficiently powering the typical features there present for O-rich and C-rich dust. Nine sources share this behavior (RAFGGL sources n. 190, 809, 865 and 954; IRC+60144; RU Vir; CIT 6; CW Leo; IRC+40156). It seems, therefore, that long-term mid-IR variability is not a common property of AGB stars, but is restricted to a special class of sources, in the special evolutionary stage when most of the flux is re-radiated by circumstellar layers of one to a few hundred K. Here stellar pulsation (which is of large amplitude in the optical bands) should effectively transfer energy to dust shells, which are quite opaque down to the mentioned temperatures. One can guess that this is the phase where the coupling between the photosphere and the circumstellar envelope is most efficient: for bluer sources, not enough dust is created, probably by a mass loss rate which is still not strong enough. For

redder objects, circumstellar dust becomes cold and distant, probably detaching itself from the central star.

One might a priori argue that the Semiregular sources might look stable only because of their small IR fluxes: when the flux is very low any variability might be more difficult to disentangle from the background noise. In order to make our suggestions more secure we looked for sources (both variable and non-variable) for which the ISO-SWS instrument offered repeated observations. We found a few interesting cases. Examples are presented in Figure 9 for the C-rich semiregular star S Scl and for the C-rich Mira variable V Cyg. Even looking, in the figure, only at homogeneous data sets (those from ISO, covering about 2 years) our previous suggestions seem to be confirmed. It is indeed clear that the Mira variable does vary as we mentioned, and it can also be understood how the non-variability of S Scl in mid-infrared in the time interval covered by the ISO data (at a level better than 10%) does not descend from an insufficient precision, since the minimum flux is of the order of tens of Jy.

The idea that the variable sources are those for which radiation pressure on dust grains powers mass loss suggests itself, though we can look at this only as at a tentative interpretation, because the source statistics and also the number of available points per source are rather limited. This hypothesis deserves now to be verified through modelling of the radiation transfer in the dust-condensing envelope, also to determine whether IR variability corresponds to a specific evolutionary stage, or can be encountered repeatedly (the same dilemma presented by optical Mira variability).

6. Conclusions

The data presented in this note confirm the usefulness of mid-IR colors taken from ground based telescopes, in describing the properties of mass-losing AGB stars. Our photometric study yields results compatible with those of Paper I, and begins to extend the analysis to a number of O-rich (S and M) sources. These will now be the object of dedicated papers, based on a large space-borne observational database similar to that of Paper I.

In general we showed how, for most semiregular variables and post-AGB stars, the IR fluxes longward of a few microns are insensitive to the variations in the stellar photosphere, and remain essentially constant in time over rather long time intervals (tens of years). This however does not apply to Mira variables, and in general to AGB sources having their maximum emission near $10\ \mu\text{m}$. Such objects show remarkable variability in the emission/absorption features (with changes from emission to absorption and back) and/or in the global flux, showing that warm dust quickly reacts to the large-amplitude surface pulsations, with large changes in concentration and temperature. This might suggest that dust-driven winds are mainly associated to the Mira stage, a hypothesis to be further verified.

Our results also point out how urgent it is to match stellar evolutionary codes with reliable model atmospheres, especially for carbon stars, including molecular opacities. This would allow one to predict reliably the effective temperature of C-rich atmospheres and hence to give a quantitative meaning to the IR color excess in terms of dust emission, without remaining uncertainties from poorly understood photospheric opacities.

Acknowledgements.

M.B. and R.G. acknowledge support by MIUR (contract PRIN2004-025729) and by PNRA (within the IRAIT project). R.G. acknowledges the University of Perugia for a

post-doc fellowship. TIRCAM2 was operated by IASF-CNR and by the Observatory of Torino (both are now part of INAF). A special thank goes to A. Ferrari, for supporting the TIRCAM2 project during his term as a director of the Torino Observatory.

This research made use of the SIMBAD database, of the VizieR service (CDS, Strasbourg, France) and of the Astrophysics Data System of NASA. In particular, archived data from the experiments MSX, ISO-SWS and 2MASS were used. [The processing of the science data from the Midcourse Space Experiment (MSX) was funded by the US Ballistic Missile Defense Organization with additional support from the NASA Office of Space Science. The Infrared Space Observatory (ISO) was an ESA project with instruments funded by ESA Member States (especially the PI countries: France, Germany, the Netherlands and the United Kingdom) and with the participation of ISAS and NASA. The Two-Micron All-Sky Survey (2MASS) was a joint project of the University of Massachusetts and of the Infrared Processing and Analysis Center (IPAC) at the California Institute of Technology; it was funded by NASA and by the NSF (USA)].

BIBLIOGRAFIA

- Bergeat, J., Knapik, A., & Rutily, B. 2001, A&A, 369, 178
- Bergeat, J., Knapik, A., & Rutily, B. 2002a, A&A, 390, 967
- Bergeat, J., & Chevallier, L. 2005, A&A, 429, 235
- Bessell, M.S., Castelli, F., & Plez, B. 1998, A&A, 333, 231
- Busso, M. 2007, in "Why Galaxies Care for AGB Stars", ed. F. Kerschbaum, C. Charbonnel, & R. Wing, ASP Conf. Series (in press)
- Busso, M., Gallino, R., & Wasserburg, G.J. 1999, ARA&A, 37, 239
- Busso, M., Tosti, G., Dolci, M., Straniero, O., & Abia, C. 2006, in "Workshop on Wide Field Imaging at Dome C", Paris, June 2006 (in press)
- Cioni, M.-R.L., Marquette, J.-B., Loup, C., et al. 2001, A&A, 377, 945
- Cioni, M.-R.L., Blommaert, J.A.D.L., Groenewegen, M.A.T., et al. 2003, A&A, 406, 51
- Cohen, M., Walker, R.G., Carter, B., et al. 1999, AJ, 117, 1864
- Corcione, L., Busso, M., Porcu, F., et al. 2003, Mem.S.A.It, 74, 57
- Cutri, R.M., Skrutskie, M.F., van Dyk, S., et al. 2003, "VizieR On-line Data Catalog: II/246", University of Massachusetts and Infrared Processing and Analysis Center, (IPAC/California Institute of Technology), 2003
- Feast, M.W., Whitelock, P.A., Menzies, P.A. 2006, MNRAS, 369, 383
- Feast, M.W. 2007, in "Why Galaxies Care for AGB Stars", ed. F. Kerschbaum, C. Charbonnel, & R. Wing, ASP Conf. Series (in press)

- Groenewegen, M.A.T., & de Jong, T. 1998, *A&A*, 337, 797
- Groenewegen, M.A.T., Sevenster, M., Spoon, H.W.W., & Pérez I. 2002, *A&A*, 390, 511
- Guandalini, R., Busso, M., Ciprini, S., Persi, P., & Silvestro, G. 2006a, *A&A*, 445, 1069
(Paper I)
- Guandalini, R., Busso M., & Cardinali, M. 2007, in "Why Galaxies Care for AGB Stars",
ed. F. Kerschbaum, C. Charbonnel, & R. Wing, ASP Conf. Series (in press)
- Habing, H.J. 1996, *A&ARv*, 7, 97
- Herwig, F. 2005, *ARA&A*, 43, 435
- Hony, S., Tielens, A.G.G.M., Waters, L.B.F.M., & de Koter, A. 2003, *A&A*, 402, 211
- Jura, M. 1986, *ApJ*, 303, 327
- Jura, M., & Kleinmann, S.G. 1989, *ApJ*, 341, 359
- Kwok, S., Volk, K., & Hrivnak, B.J. 1999, in "Asymptotic Giant Branch Stars", IAU
Symposium 191, ed. T. Le Bertre, A. Lebre, & C. Waelkens, 297
- Kwok, S., Volk, K.M., & Hrivnak B.J. 2002, *ApJ*, 573, 720
- Le Bertre, T., Matsuura, M., Winters, J.M., et al. 2001, *A&A*, 376, 997
- Le Bertre, T., Tanaka, M., Yamamura, I., & Murakami, H. 2003, *A&A*, 403, 943
- Le Bertre, T., Tanaka, M., Yamamura, I., Murakami, H., & MacConnell, D.J. 2005, *PASP*,
117, 199
- Leech, K., Kester, D., Shipman, R. et al. 2004, *The ISO Handbook*, Volume V. SWS:
The Short Wavelength Spectrometer, Version 2.0.1, ed. T. Müller & J. Blommaert
(Noordwijk:ESA)

- Loidl, R., Lançon, A., & Jørgensen, U.G. 2001, *A&A*, 371, 1065
- Loup, C., Forveille, T., Omont, A., & Paul, J.F. 1993, *A&AS*, 99, 291
- Marigo, P., Bressan, A., & Chiosi, C. 1998, *A&A*, 331, 564
- Marigo, P. 2007, *A&A*, (in press)
- Meixner, M., Campbell, M.T., Welch, W.J., & Likkell, L. 1998, *ApJ*, 509, 392
- Men'shchikov, A.B., Schertl, D., Tuthill, P.G., et al. 2002, *A&A*, 393, 867
- Menzies, J.W., Feast, M.W., & Whitelock, P.A. 2006, *MNRAS*, 369, 783
- Olofsson, H., Eriksson, K., Gustafsson, B., & Carlstrom, U. 1993a, *ApJS*, 87, 267
- Olofsson, H., Eriksson, K., Gustafsson, B., & Carlstrom, U. 1993b, *ApJS*, 87, 305
- Persi, P., Ferrari-Toniolo, M., Marenzi, A.R., et al. 1994, *Exp. Astron.*, 5, 363
- Persi, P., Busso, M., Corcione, L., et al. 2002, *SIF Conf. Proc. "Solids and Molecules in Space"*, vol.77, p.205
- Sedlmayr, E. 1994, *Lecture Notes in Physics*, 428, 163
- Stetson, P.B. 1987, *PASP*, 99, 191
- Straniero, O., Chieffi, A., Limongi, M., et al. 1997, *ApJ*, 478, 332
- Straniero, O., Domínguez, I., Cristallo, S., & Gallino, R. 2003, *PASA*, 20, 389
- Tosti, G., Busso, M., Nucciarelli, G., et al. 2006, *SPIE*, 6267, 47.
- Uttenthaler, S., Hron, J., Lebzelter, T., Busso, M., Shultheis, M., & Käufl, H.-U. 2006, *A&A*, (in press: astro-ph/0610500)

van Leeuwen, F. 2005, *A&A*, 439, 805

van Leeuwen, F., & Fantino, E. 2005, *A&A*, 439, 791

van Loon, J.Th., Groenewegen, M.A.T., de Koter, A., et al. 1999, *A&A*, 351, 559

van Loon, J.Th., Zijlstra, A.A., Kaper, L., et al. 2001, *A&A*, 368, 239

van Loon, J.Th., Cioni, M.-R.L., Zijlstra, A.A., & Loup, C, 2005, *A&A*, 438, 273

Whitelock, P.A., Feast, M.W., Marang, F., & Groenewegen, M.A.T. 2006, *MNRAS*, 369, 751

Winters, J.M., Le Bertre, T., Nyman, L.-Å., et al. 2002, *A&A*, 388, 609

Winters, J.M., Le Bertre, T., Jeong, K.S., et al. 2003, *A&A*, 409, 715

Zhang, K., Jiang, B.-W. & Li, A.-G. 2006, *P.A. Bei*, 24, 43

Zijlstra, A.A., Matsuura, M., Wood, P.R., Sloan, G.C., Lagadec, E., et al. 2006, *MNRAS*, 370, 1961

FIGURE CAPTIONS

Figura 1 An example of a color-color diagram for the observed stars. Big symbols are from TIRCAM2, small ones from Paper I. See text for comments.

Figura 2 Another example of a color-color diagram for the observed stars. Again, big symbols are from TIRCAM2, small ones from Paper I. See text for explanations.

Figura 3 Mass loss rates as a function of the infrared colors for the sample of stars in this paper (large dots) and for the best-measured sources of Paper I (small dots). As usual, open symbols refer to S stars, filled symbols to C stars.

Figura 4 The color-magnitude diagram for our sources, using the J-K color as a temperature indicator (see text for explanations). Small symbols are from Paper I. The "C-star limit" line refers to $2 M_{\odot}$ models of solar metallicity.

Figura 5 Same as above, but using the K-[12.5] color in abscissa. This color samples dust of different temperatures (and also, in K, the residual photospheric flux); the horizontal extension of the data is a measure of the infrared excess due to the dusty envelope.

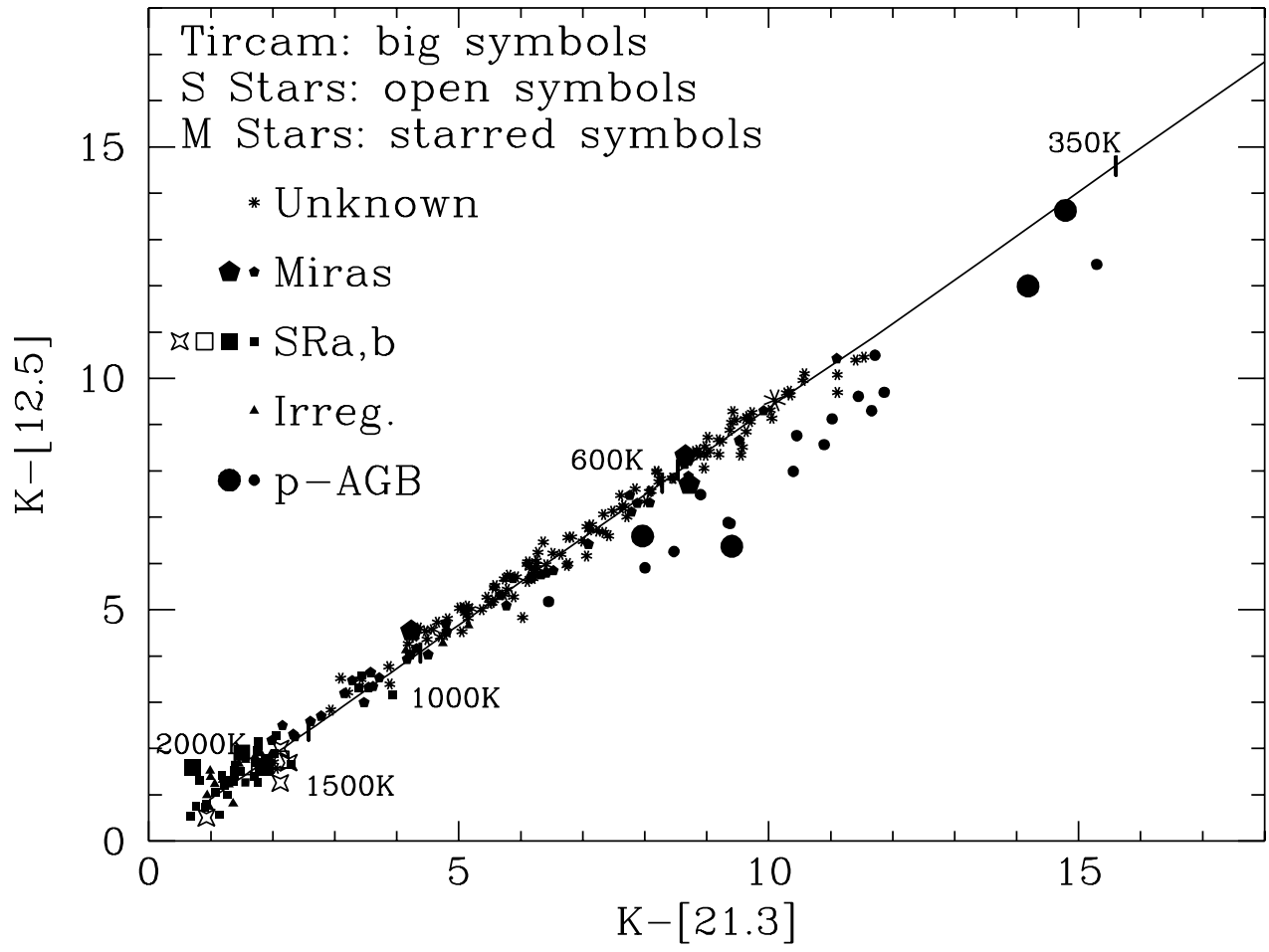
Figura 6 The HR diagram of the few TIRCAM2 C-rich (full large dots) or S-type (open large symbols) stars for which we could find in the literature independent estimates of T_{eff} . For S-stars T_{eff} is an extrapolation [from the relations by Bessell et al. 1998]. Small symbols refer to those C-rich stars from Paper I having astrometric distances and values of T_{eff} . The curves at the right are from the AGB models at various masses and metallicities [Straniero et al. 2003]. It is evident that, on average, C-rich sources show large temperature discrepancies compared to models sequences. The curves on the right side are shifted by 0.1dex in $Log T_{eff}$, in order to mimic molecular opacity effects [Marigo 2007].

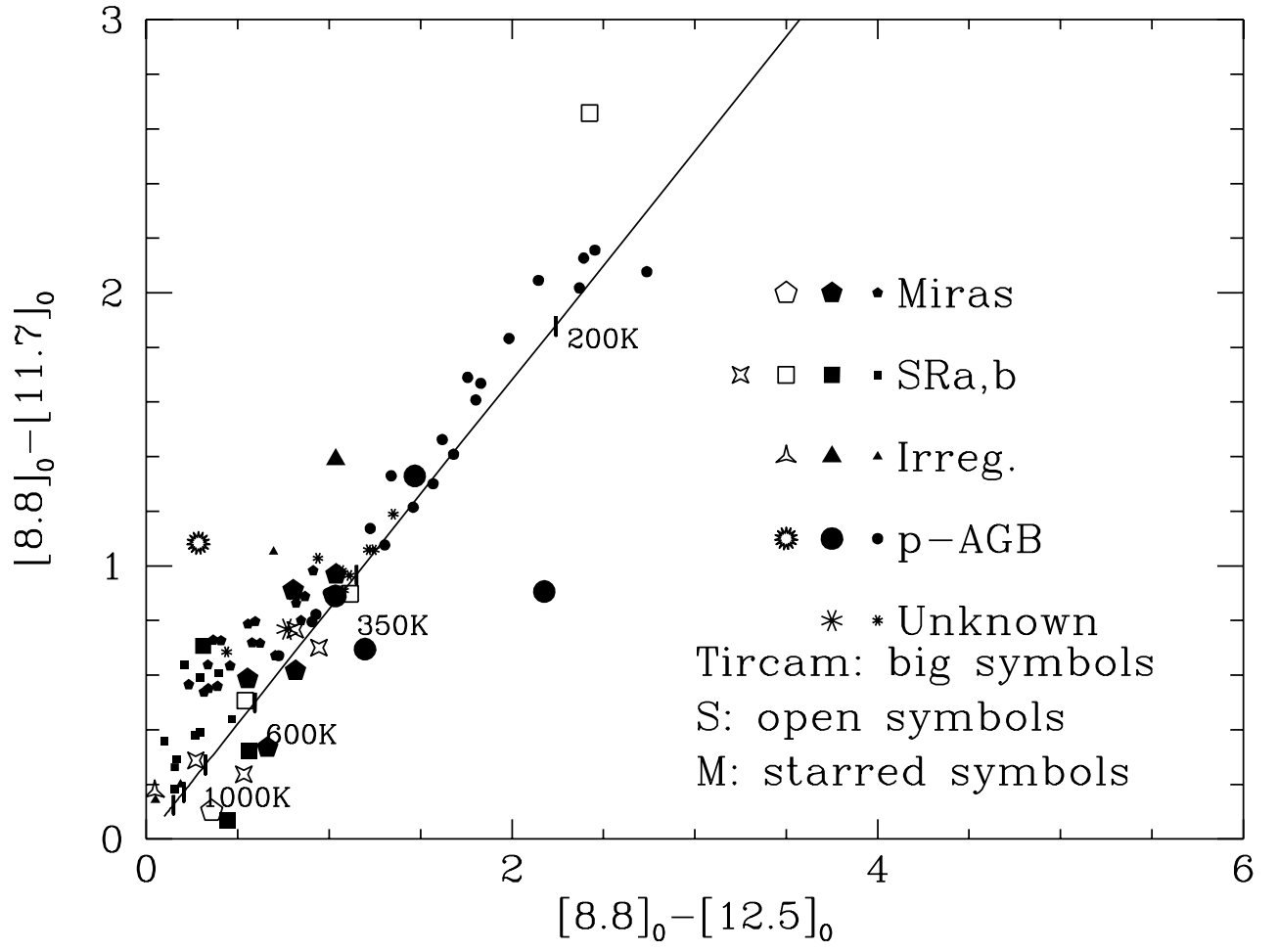
Figura 7 The Spectral Energy Distributions of a few non-variable sources, as available from

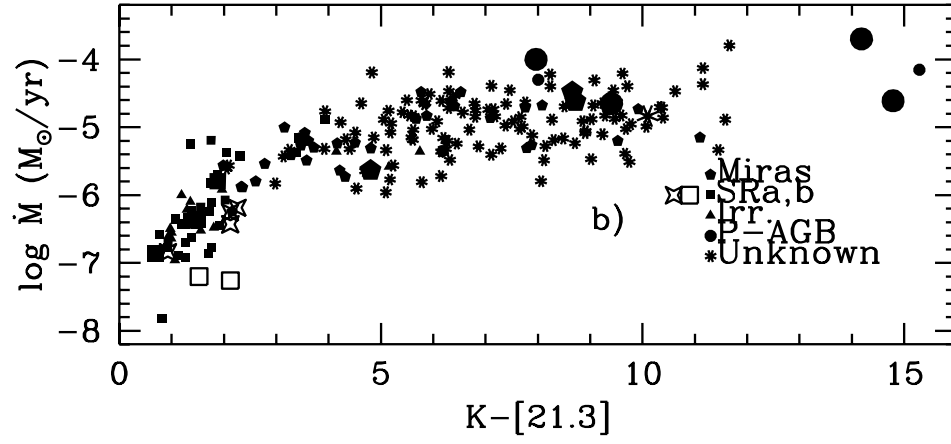
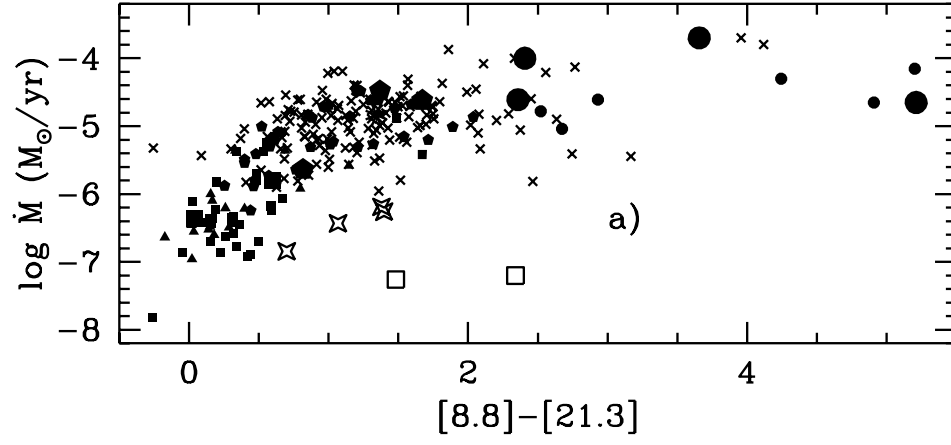
our TIRCAM2 observations and from the IRAS PSC, IRAS LRS, ISO-SWS, MSX, and 2MASS catalogues. SEDs with maximum emission in the near-infrared, as well as those with maximum emission longward of $20\mu\text{m}$ all show a constant flux in mid-IR.

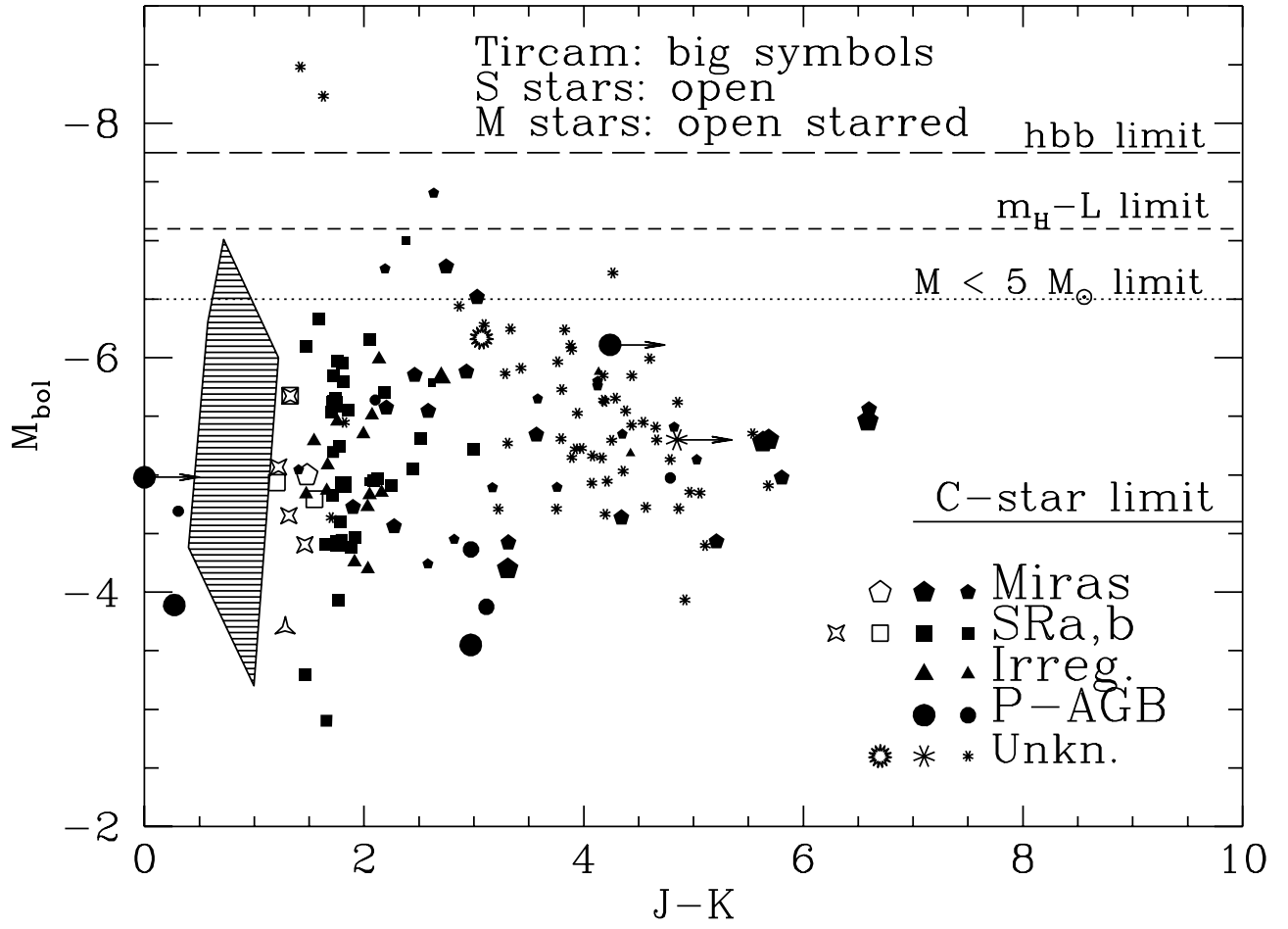
Figura 8 Spectral Energy Distributions of sources that show significant variability over the time elapsed from the IRAS to the TIRCAM2 observations. Again, data obtained with TIRCAM2 and data available from the IRAS PSC, IRAS LRS, ISO-SWS, MSX, and 2MASS catalogues are included. Only sources for which the emission is maximum in the range $8 - 20\mu\text{m}$ do appear to be variable, independently on their composition (C-rich or O-rich).

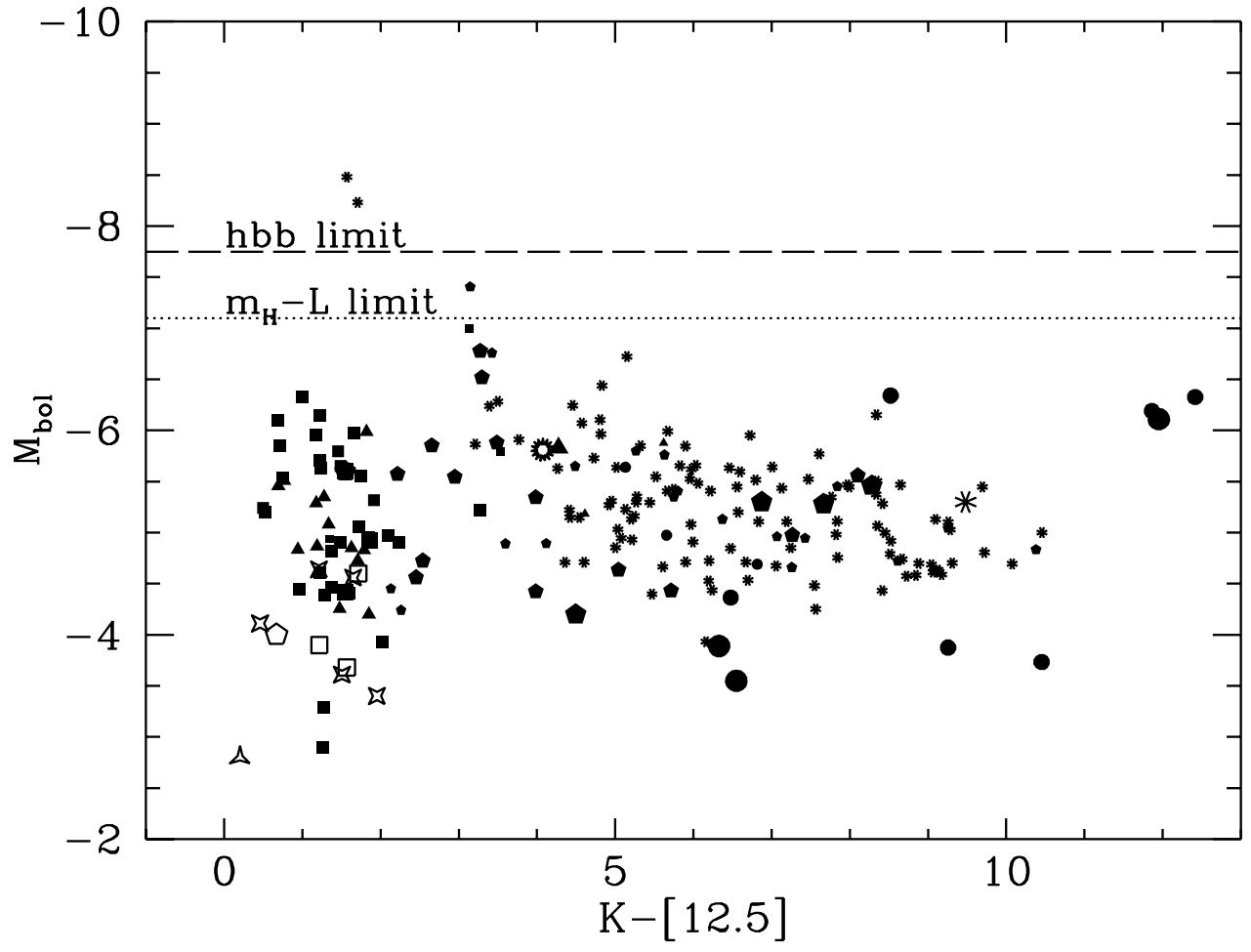
Figura 9 ISO-SWS Spectral Energy Distributions of two Carbon Stars: a Mira variable (top panel) and a Semiregular (bottom panel); they were observed repeatedly by ISO during about 2 years. On this rather short time scale, but with homogeneous data, our suggestions about mid-IR variability of Miras and flux constancy of Semiregulars seem to be confirmed.

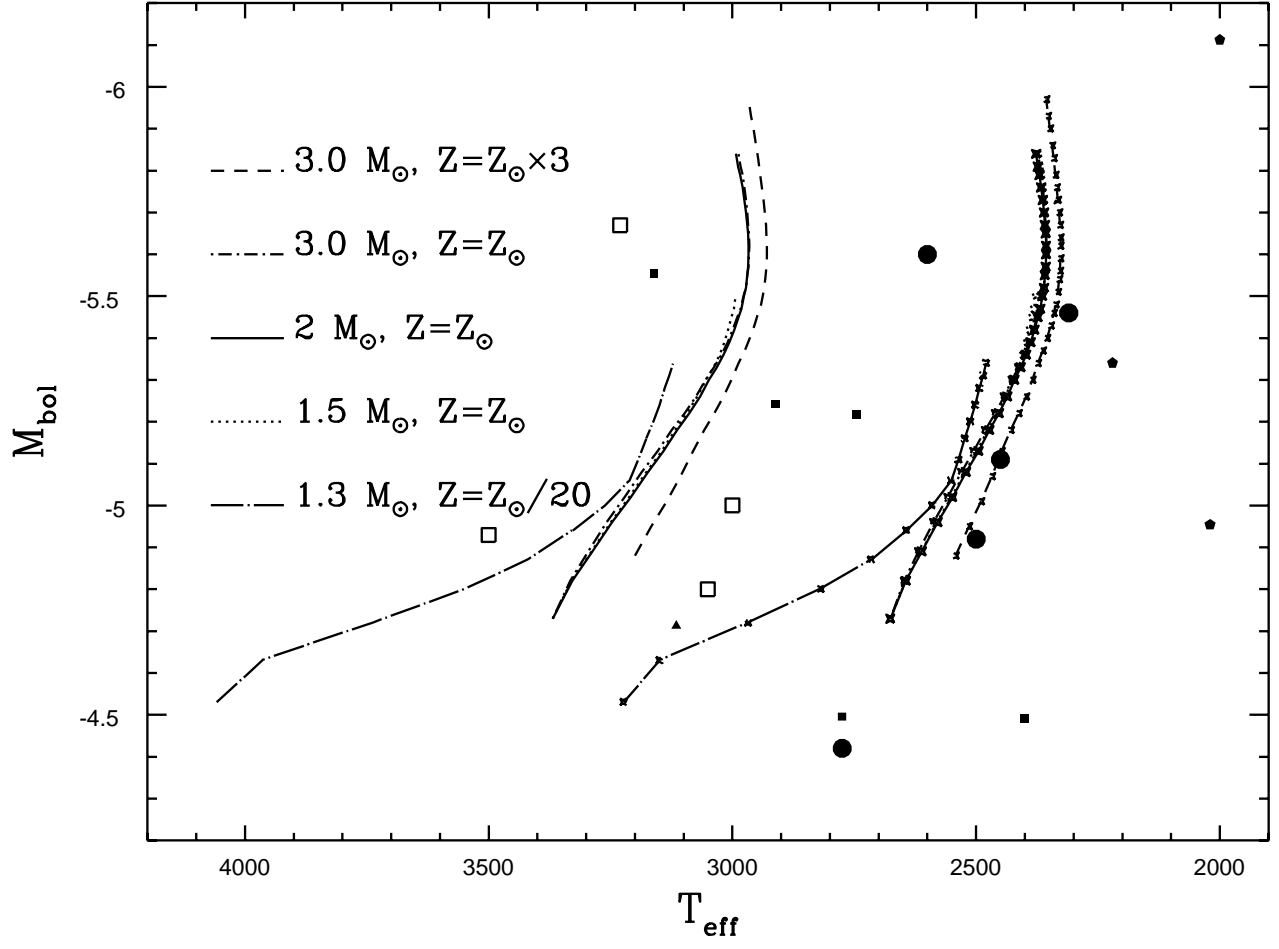


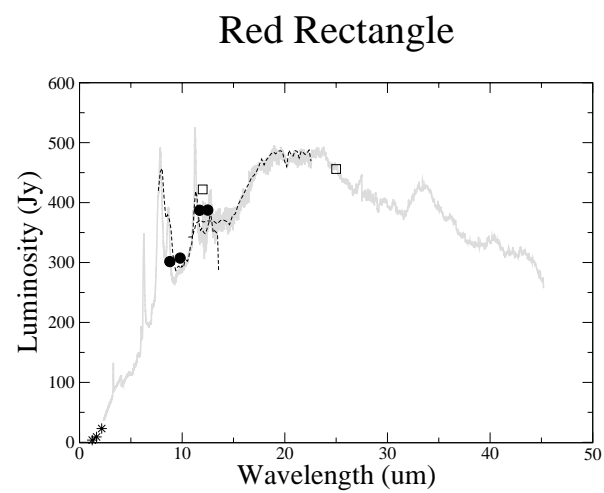
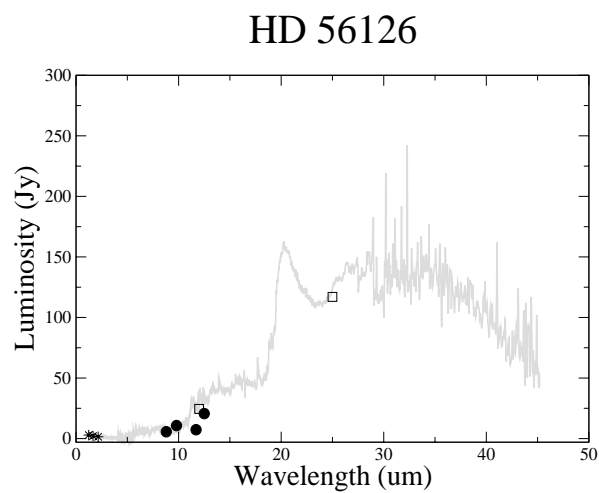
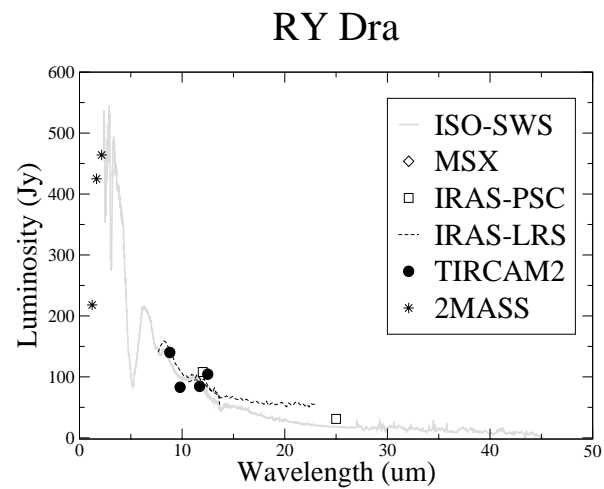
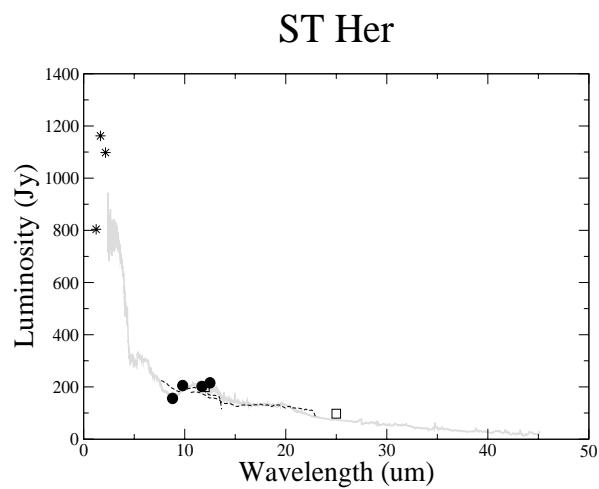


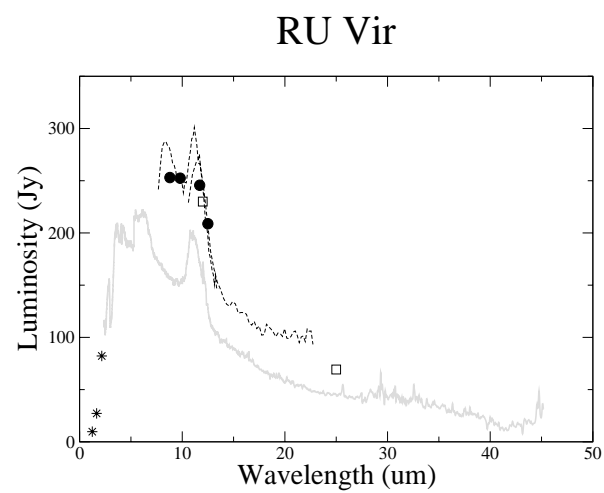
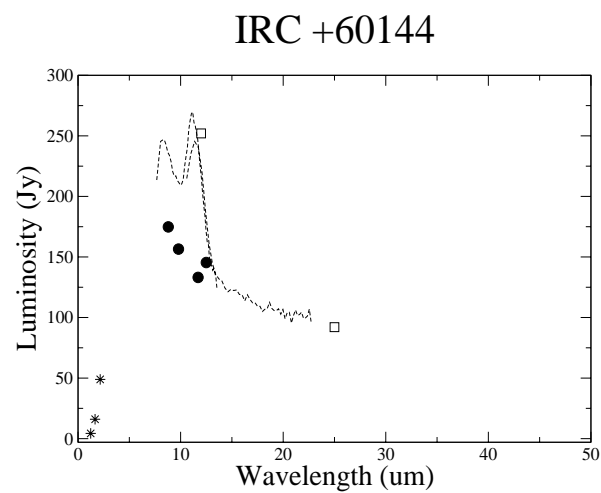
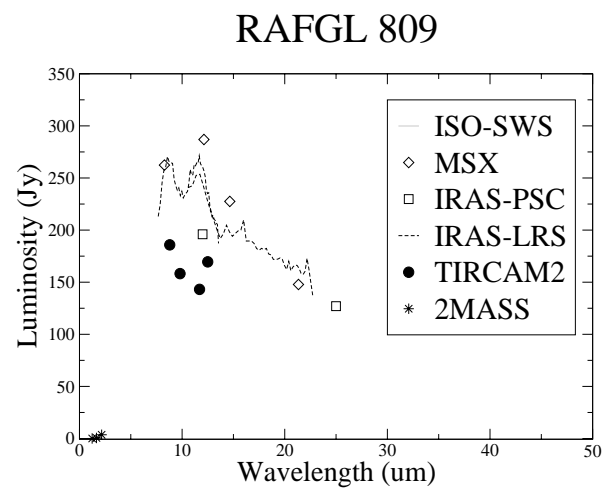
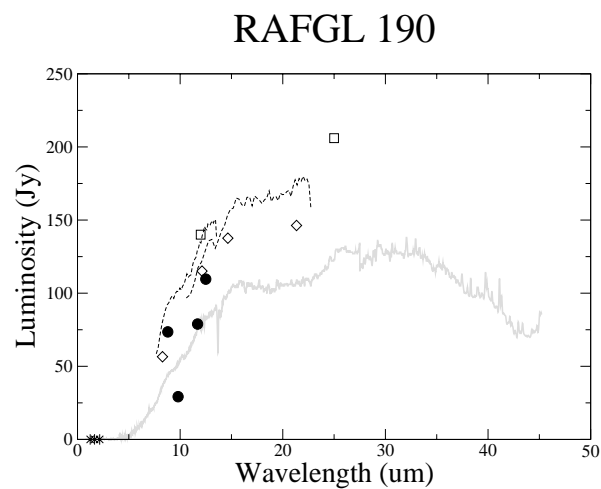




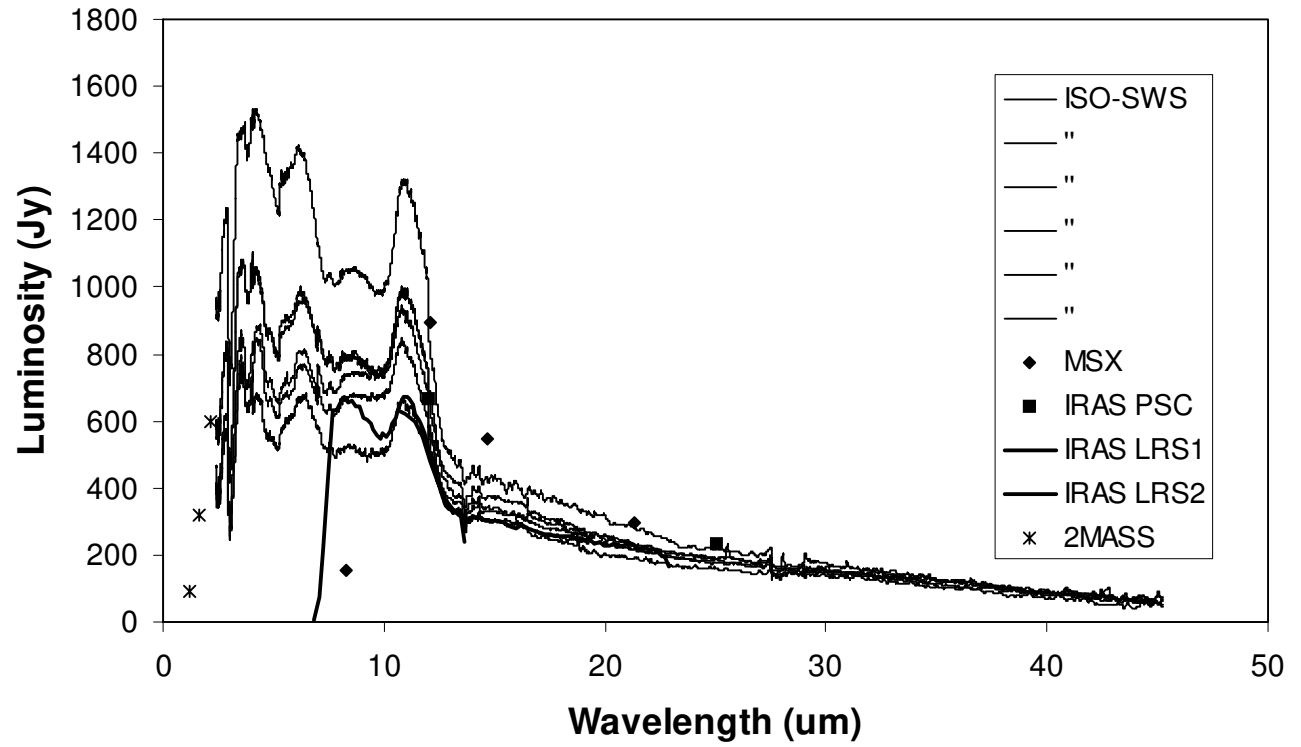








V Cyg



R Scl

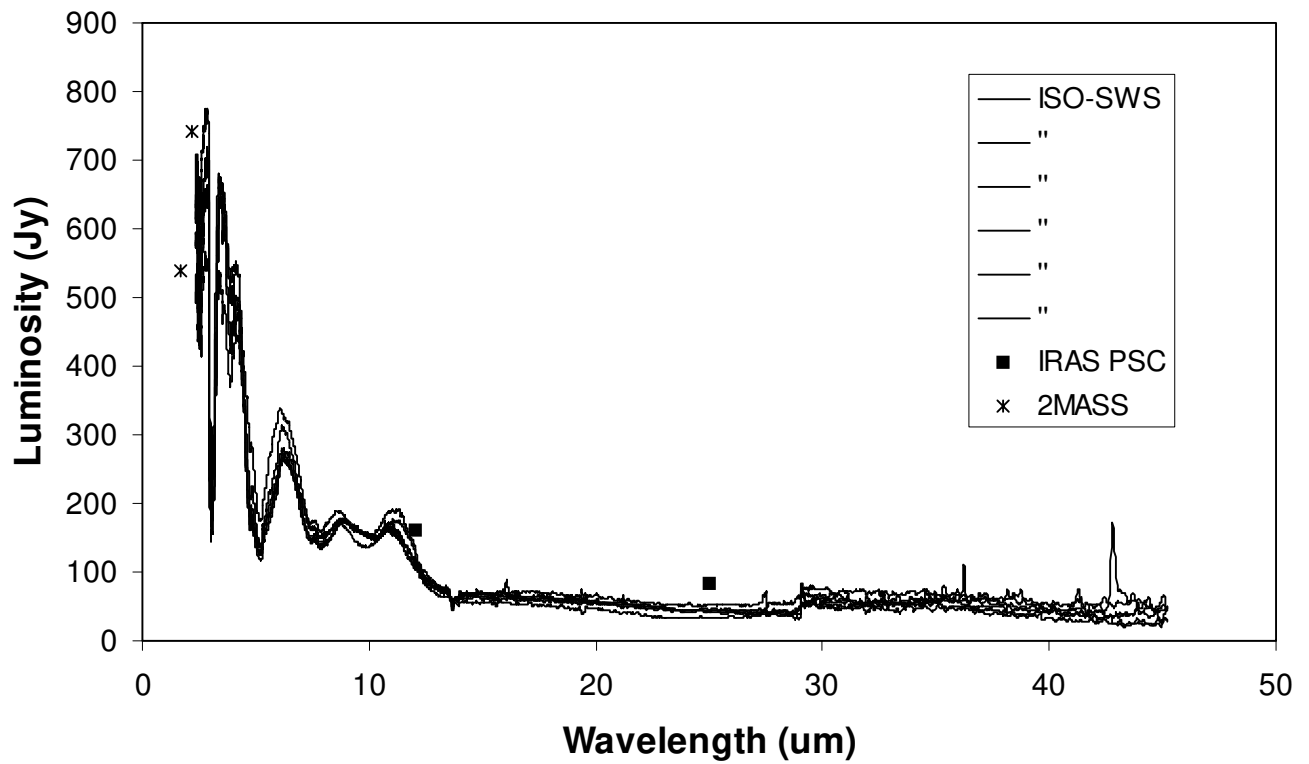


Tabella 1 The TIRCAM2 Sample of AGB Stars.

Number	IRAS Name	Other Name	Coordinates	Var. Type	Type
1	01144+6658	RAFGL 190	01 17 51.62 +67 13 55.4	P	C
2	03186+7016	RAFGL 482	03 23 36.57 +70 27 07.5	M	C
3	04307+6210	IRC +60144	04 35 17.45 +62 16 23.3	S	C
4	04395+3601	RAFGL 618	04 42 53.67 +36 06 53.2	P	C
5	04530+4427	RAFGL 6319S	04 56 43.28 +44 32 41.6	–	C
6	05405+3240	RAFGL 809	05 43 49.78 +32 42 06.8	M	C
7	05426+2040	Y Tau	05 45 39.41 +20 41 42.1	S	C
8	06012+0726	RAFGL 865	06 03 59.84 +07 25 54.4	M	C
9	06176–1036	Red Rectangle	06 19 58.22 -10 38 14.7	P	C
10	06291+4319	RAFGL 954	06 32 41.93 +43 17 15.3	I	C
11	07134+1005	HD 56126	07 16 10.26 +09 59 48.0	P	C
12	09452+1330	CW Leo	09 47 57.38 +13 16 43.7	M	C
13	10131+3049	CIT 6	10 16 02.27 +30 34 18.6	S	C
14	12427+4542	Y CVn	12 45 07.83 +45 26 24.9	S	C
15	12447+0425	RU Vir	12 47 18.41 +04 08 41.4	M	C
16	12544+6615	RY Dra	12 56 25.91 +65 59 39.8	S	C
17	06331+1415	DY Gem	06 35 57.81 +14 12 46.1	S	S
18	09076+3110	RS Cnc	09 10 38.80 +30 57 47.3	S	S
19	12417+6121	S UMa	12 43 56.68 +61 05 35.5	M	S
20	15492+4837	ST Her	15 50 46.62 +48 28 58.9	S	S
21	06297+4045	IRC +40156	06 33 15.75 +40 42 50.9	P	M
22	12277+0441	BK Vir	12 30 21.01 +04 24 59.2	S	M
23	13001+0527	RT Vir	13 02 37.98 +05 11 08.4	S	M
24	14059+4405	BY Boo	14 07 55.76 +43 51 16.0	I	M
25	14219+2555	RX Boo	14 24 11.63 +25 42 13.4	S	M
26	14371+3245	RV Boo	14 39 15.86 +32 32 22.3	S	M
27	16269+4159	g Her	16 28 38.55 +41 52 54.0	S	M

Tabella 2 Flux Densities of standard stars.

Standard	[8.8]	[9.8]	[11.7]	[12.5]
	(Jy)	(Jy)	(Jy)	(Jy)
α Lyr	49.69	40.44	28.48	25.05
β Gem	152.74	120.90	88.67	76.77
α Boo	883.72	745.32	524.94	459.01
β And	306.36	263.52	200.79	174.55
β Peg	431.12	376.00	279.25	249.01
α Tau	752.09	646.86	481.44	419.57

Tabella 3 Our TIRCAM2 observations in the $10\mu\text{m}$ window.

Source Number	Epoch	F[8.8] (Jy)	F[9.8] (Jy)	F[11.7] (Jy)	F[12.5] (Jy)
1	16.1.2003	73.5(5.4)	29.2(8.2)	78.9(11.3)	109.6(14.4)
2	16.1.2003	147.1(7.9)	—	146.8(17.6)	154.6(19.1)
3	16.1.2003	174.8(8.8)	156.5(10.9)	133.1(16.4)	145.4(19.2)
4	6.12.2003	254.6(27.1)	380.2(42.8)	490.2(26.7)	488.0(28.4)
5	13.2.2002	87.2(19.1)	83.0(8.3)	100.1(10.0)	87.8(9.0)
6	16.1.2003	185.8(9.3)	158.2(11.9)	143.1(17.5)	169.5(21.5)
7	12.2.2002	122.6(13.5)	116.8(7.4)	133.0(6.7)	80.9(3.6)
8	6.12.2003	364.9(28.9)	414.1(41.1)	477.9(34.6)	379.1(43.2)
9	7.12.2003	301.5(34.2)	307.5(50.4)	387.2(35.9)	387.4(49.0)
10	15.1.2003	63.4(6.6)	66.2(14.6)	129.1(12.6)	81.6(24.)
11	6.2.2004	5.6(1.8)	10.7(2.4)	7.3(2.8)	20.6(2.7)
12	14.1.2001	30255.(605.)	—	41782.(342.)	38978.(667.9)
13	15.1.2003	1789.(156.)	1976.(190.)	2226.(400.)	
14	6.12.2003	342.8(20.3)	337.0(29.0)	108.9(22.0)	220.7(24.6)
15	16.1.2003	253.0(27.6)	252.4(24.3)	245.7(39.3)	208.8(25.5)
16	16.1.2003	140.1(15.7)	83.0(10.7)	84.4(13.8)	104.4(13.4)
17	6.2.2004	5.3(1.6)	16.4(3.3)	34.7(10.5)	24.5(4.5)
18	14.1.2001	398.4(40.0)	550.0(82.5)	453.1(63.4)	378.3(57.0)
”	11.2.2002	568.5(47.8)	790.7(29.8)	497.2(13.0)	452.1(33.0)
”	6.12.2003	570.0(30.0)	739.1(49.0)	530.0(37.0)	477.1(28.0)
19	11.2.2002	4.5(0.5)	—	2.8(0.5)	3.1(0.7)
20	4.2.2004	155.7(8.0)	205.2(33.0)	201.4(50.0)	215.5(28.0)
21	15.1.2003	209.4(10.8)	334.1(37.8)	321.4(69.0)	134.9(10.0)
22	4.2.2004	224.6(11.3)	217.6(32.6)	118.4(29.6)	211.6(27.5)
23	14.1.2001	365.7(16.4)	496.4(24.0)	394.3(22.4)	432.5(54.3)
24	12.2.2002	77.7(8.6)	72.2(1.3)	51.6(2.6)	40.2(2.3)
25	11.2.2002	694.8(58.4)	922.2(34.7)	795.8(20.5)	729.2(52.9)
26	6.2.2004	106.7(13.9)	151.3(47.2)	75.1(21.0)	86.4(8.6)
27	12.2.2002	461.6(50.9)	427.4(27.0)	340.4(17.3)	293.6(13.2)

Tabella 4 Source fluxes in the 2MASS, MSX & ISO filters (Jy)

Source no.	Var. type	J	H	K	14,6	21,3	Data orig.
1	P	0.01	0.02	0.01	96.3	110	ISO
2	M	0.09	1.1	6.8	—	—	—
3	S	4.3	16.0	48.9	—	—	—
4	P	< 0.01	0.03	0.20	651	1260	ISO
5	—	< 0.01	0.03	0.35	62.0	51.2	MSX
6	M	0.05	0.53	3.6	227.5	147.8	MSX
7	S	242	495	481	59.1	36.4	MSX
8	M	< 0.01	0.20	2.5	—	—	—
9	P	3.7	9.0	23.0	377	472	ISO
10	I	8.1	22.7	39.3	—	—	—
11	P	2.9	2.1	1.5	42.0	116	ISO
12	M	2.7	74.9	469	26309	18194	ISO
13	S	2.5	17.1	91.4	—	—	—
14	S	641	1331	1316	53.8	33.5	ISO
15	M	9.7	27.2	82.2	91.6	54.3	ISO
16	S	218	425	464	50.4	24.7	ISO
17	S	85.4	156	143	12.7	7.8	MSX
18	S	3065	4324	3743	—	—	—
19	M	26.3	43.4	41.4	—	—	—
20	S	804	1162	1098	149	104	ISO
21	P	11.5	33.8	78.3	—	—	—
22	S	966	1448	1306	—	—	—
23	S	1145	1843	1770	—	167	ISO
24	I	630	1033	826	—	—	—
25	S	—	4210	3948	584	422	ISO
26	S	512	785	700	76	66	ISO
27	S	3841	5627	4760	273	150	ISO

Tabella 5 Relevant parameters and distances of the sample stars.

Source no.	Var. type	\dot{M} [M_{\odot}/yr]	Type (ref.)	v [km/s]	d [kpc]	Type ref.
1	P	2.45E-05	L	18.2	2.79	G
2	M	1.05E-05	L	12.2	1.97	G
3	S	6.33E-06	L	18.5	1.03	G
4	P	2.00E-04	Mei1998	19.5	1.70	Mei1998
5	—	1.46E-05	L	20.2	2.60	G
6	M	2.40E-05	L	28.0	2.01	G
7	S	1.60E-06	B	11.0	0.74	B
8	M	1.16E-05	L	15.8	1.47	G
9	P	1.00E-04	Men2002	5.0	0.71	Men2002
10	I	6.37E-06	L	21.4	2.19	G
11	P	2.23E-05	L	10.7	2.40	Hon2003
12	M	3.30E-05	B	14.7	0.15	B
13	S	6.50E-06	B	17.0	0.41	B
14	S	1.40E-07	B	8.5	0.26	B
15	M	2.30E-06	B	18.4	0.68	B
16	S	4.40E-07	B	10.0	0.55	B
17	S	6.27E-08	G-dJ	8.0	0.56	G-dJ
18	S	3.92–5.20E-08	G-dJ	7.2	0.12	Hip
19	M	—	—	—	1.15	G-dJ
20	S	4.52–7.21E-08	G-dJ	9.1	0.31	Hip
21	P	1.00E-05	L	16.3	1.60	L
22	S	5.49E-07	W	7.5	0.18	Hip
23	S	3.70E-07	L	9.3	0.14	Hip
24	I	—	—	—	0.14	Hip
25	S	6.48E-07	L	10.2	0.16	Hip
26	S	5.49E-07	L	8.1	0.39	Hip
27	S	1.43E-07	L	8.5	0.11	Hip